

Vitrimer Elastomer-Based Jigsaw Puzzle-Like Healable Triboelectric Nanogenerator for Self-Powered Wearable Electronics

Jianan Deng, Xiao Kuang, Ruiyuan Liu, Wenbo Ding, Aurelia C. Wang, Ying-Chih Lai, Kai Dong, Zhen Wen, Yaxian Wang, Lili Wang, H. Jerry Qi,* Tong Zhang,* and Zhong Lin Wang*

Functional polymers possess outstanding uniqueness in fabricating intelligent devices such as sensors and actuators, but they are rarely used for converting mechanical energy into electric power. Here, a vitrimer based triboelectric nanogenerator (VTENG) is developed by embedding a layer of silver nanowire percolation network in a dynamic disulfide bond-based vitrimer elastomer. In virtue of covalent dynamic disulfide bonds in the elastomer matrix, a thermal stimulus enables in situ healing if broken, on demand reconfiguration of shape, and assembly of more sophisticated structures of VTENG devices. On rupture or external damage, the structural integrity and conductivity of VTENG are restored under rapid thermal stimulus. The flexible and stretchable VTENG can be scaled up akin to jigsaw puzzles and transformed from 2D to 3D structures. It is demonstrated that this self-healable and shape-adaptive VTENG can be utilized for mechanical energy harvesters and self-powered tactile/pressure sensors with extended lifetime and excellent design flexibility. These results show that the incorporation of organic materials into electronic devices can not only bestow functional properties but also provide new routes for flexible device fabrication.

next-generation wearable medical and security devices. Various flexible components have been designed, such as transistors,^[1] sensors,^[2] supercapacitors,^[3] solar cells,^[4] and so on. Most electronic devices rely on electricity, which is typically supplied by the energy stored in batteries and capacitors. For wearable devices that are suitable for human usage, miniaturization and weight reduction are essential design factors. In this case, energy storage units should avoid being large in size, in effect deviating from the paramount goal of powering long-term operation. Hence, stable and sustainable power supply is highly desirable for constant recharging of an energy storage unit.

In wearable electronic systems, the ideal energy source would be mechanical energy from human motion. Traditional electromagnetic generators are not suitable for being deployed as wearable

As technology advances, consumers are no longer satisfied with rigid wearable electronic devices, as traditionally stiff constituents are being replaced by flexible components. Their remarkable conformability and stretchability can provide a seamless and comfortable experience for human-machine interaction, which are considered as a key element for the

mechanical energy harvesters due to their heavy weight, bulky volume, and inflexibility. However, a recently emerging triboelectric nanogenerator (TENG) technology that is based on contact electrification and electrostatic induction is a promising candidate. It has the capability to harvest different forms of energy from the ambient environment including wind,^[5]

Dr. J. Deng, Dr. R. Liu, Dr. W. Ding, A. C. Wang, Dr. Y.-C. Lai, K. Dong, Dr. Z. Wen, Dr. Y. Wang, Prof. Z. L. Wang
School of Materials Science and Engineering
Georgia Institute of Technology
Atlanta, GA 30332, USA
E-mail: zhong.wang@gatech.edu

Dr. J. Deng, Dr. L. Wang, Prof. T. Zhang
State Key Laboratory on Integrated Optoelectronics
College of Electronic Science and Engineering
Jilin University
Changchun 130012, P. R. China
E-mail: zhangtong@jlu.edu.cn

 The ORCID identification number(s) for the author(s) of this article can be found under <https://doi.org/10.1002/adma.201705918>.

Dr. X. Kuang, Prof. H. J. Qi
George W. Woodruff School of Mechanical Engineering
Georgia Institute of Technology
Atlanta, GA 30332, USA
E-mail: qih@me.gatech.edu

Dr. R. Liu, Dr. Z. Wen
Institute of Functional Nano and Soft Materials
Soochow University
Suzhou, Jiangsu 215123, P. R. China

Prof. Z. L. Wang
Beijing Institute of Nanoenergy and Nanosystems
Chinese Academy of Sciences
National Center for Nanoscience and Technology (NCNST)
Beijing 100083, P. R. China

DOI: 10.1002/adma.201705918

waves,^[6] vibration,^[7] motion,^[8] and even friction.^[9] Due to the TENG's unique working mechanism, it possesses not only adaptive architectures capable of accommodating arbitrary surfaces, but may also be scaled down to create diminutive devices and reduce unit mass.^[10] Low frequency^[11] and irregular mechanical energy can be converted into electricity through TENGs, which is particularly beneficial to harvesting energy from natural motion. The aforementioned features are all critical to wearable electronics. Based on this, a variety of flexible energy harvesters have already been fabricated.^[12] However, there still exist obstacles to implementing this technology into application, the main limitations being device durability and complicated fabrication.

Recently, self-healing materials have been developed to enable structural restoration and function recovery of materials, which can enhance reliability and extend lifetime of devices.^[13] Artificial self-healing systems fall into two categories: extrinsic self-healing polymer composites through releasing and polymerizing an encapsulated healing agent (healants) and intrinsic self-healing polymers containing dynamic covalent or noncovalent bonds. Dynamic network polymers containing sufficient reversible covalent bonds are called vitrimers, capable of rearranging the network under stimuli such as heat, light, or pH.^[14] An array of dynamic reactions, such as, Diels–Alder reaction,^[15] disulfide metathesis,^[16] imide metathesis,^[17] transesterification,^[18] and olefin metathesis^[19] have been investigated and found to achieve self-healing, reprocessing, or welding of thermosets. Compared with other dynamic covalent bonds, the dynamic disulfide bond is particularly attractive due to its unique qualities, such as, easy fabrication from commercially available starting materials in a scalable manner, and multiple stimuli-responsiveness (light, thermal, or chemical).^[20] Progress has driven many exciting applications of self-healing materials to be employed in electronic devices, such as, conductors,^[21] supercapacitors,^[22] and electronic skin^[23] with enhanced durability. However, most of the current self-healing materials for electronic devices are based on relatively weak hydrogen bonding, which suffers from poor mechanical properties and low creep resistance. The implementation of self-healing polymers with stronger covalent bonding in flexible electronics would open the path for smart, durable, freely-designable, and readily fabricated wearable electronics.^[24]

Herein, we present the first self-healable, flexible, and stretchable mechanical energy harvester and tactile sensing element, by embedding a silver nanowire network in a disulfide bond containing vitrimer elastomer. The dynamic disulfide exchange reaction in the self-healing elastomer enables fast structural/functional recovery and affords efficient shape adaptivity or configurability. Furthermore, the terrace-structured design of the self-healing device element endows the energy harvester with excellent durability, provides a new scaling up method for flexible TENG that easy like playing jigsaw puzzles and building blocks. To fabricate the vitrimer elastomer, we used commercially available starting materials to obtain an epoxy resin-based polysulfide elastomer. Briefly, bisphenol A diglycidyl ether epoxy oligomer was mixed with pentaerythritol tetrakis(3-mercaptopropionate) (as a spacer) and polysulfide oligomer (as an oligomer crosslinker) with 2,4,6-tris(dimethylaminomethyl) phenol catalyst (**Figure 1a**). The epoxy oligomer

was cross-linked with thiols in a base-catalyzed addition reaction. After curing, the nearly complete cross-linking reaction was verified by the complete disappearance of S–H stretching vibration (2536 cm^{-1}) and oxirane ring stretching vibration (916 cm^{-1}) bands in FTIR spectra (**Figure S1**, Supporting Information), indicating that the disulfide bond was incorporated into the network. The obtained material is a typical elastomer with a fracture strain over 100% (**Figure S2**, Supporting Information). It is noted that the amount of catalyst has a significant effect on mechanical properties. Through increasing the catalyst content to 3 wt%, the fracture increases from 100% to 250%. **Figure 1b** shows cyclic tensile behavior for five cycles. The unrecoverable strain (or plastic strain) was about 10% after the first cycle (0% to 50% to 0% strain). The subsequent strain cycles nearly overlap with some signs of hysteresis. In addition, the stress–strain curves of the step-cycle measurements show that the elastic deformation is dominant (**Figure S3**, Supporting Information). The glass transition temperature of the vitrimer sample was about $0\text{ }^{\circ}\text{C}$ by dynamic mechanical analysis (DMA), further indicating that the material is an elastomer (**Figure S4**, Supporting Information). These results suggest that the flexible sample shows excellent elastic properties with large fracture strain, which can be a candidate for flexible electronics matrix.

The dynamic adaptive feature of vitrimer elastomer was evaluated by the temperature-dependent stress relaxation test via DMA. **Figure 1c** shows that the normalized stress relaxation modulus gradually decreases with time at different temperatures (from 20 to $70\text{ }^{\circ}\text{C}$). Therefore, the elastomer was a vitrimer capable of relaxing stress for an extended time due to the dynamic bond exchange reaction, because the catalyst used for the curing reaction also acts as a catalyst for the dynamic reaction of disulfide metathesis. According to Maxwell's model for viscoelastic fluids, relaxation times (τ) were determined as the time required to relax to $1/e$ (36.7%) of the initial stress or modulus. The relaxation times were found to decrease sharply with increasing temperature. For example, τ is over 10^4 s at $20\text{ }^{\circ}\text{C}$, which decreases to 5 s at $70\text{ }^{\circ}\text{C}$. The relaxation activation energy was calculated to be 146 kJ mol^{-1} fitted by the Arrhenius' law (Equation (S1) and **Figure S5**, Supporting Information). The relaxation activation energy (E_a) reflects the reaction activation energy of disulfide exchange reaction.^[25] High E_a value suggests that dynamic disulfide metathesis is sensitive to temperature using the above catalyst, which shows several advantages for practical application. On one hand, the large τ affords necessary size-stability and elasticity at low temperature. On the other hand, the small τ at elevated temperatures affords fast responsiveness for functional properties such as self-healing and shape adaptive.

The dynamic disulfide bond enables self-healing capability of the vitrimer elastomer. The mechanical healing performance was evaluated by tensile tests and the healing efficiency was quantitatively calculated by the recovery of fracture strain (Equation (S2), Supporting Information). **Figure 1d** shows the typical stress–strain curves of the original and healed samples at $65\text{ }^{\circ}\text{C}$ for different healing time. Better recovery was obtained using longer healing times with nearly 100% recovery after healing at $65\text{ }^{\circ}\text{C}$ for 4 h. Higher healing temperatures also contributed to better healing. As shown in **Figure 1e**, with a healing

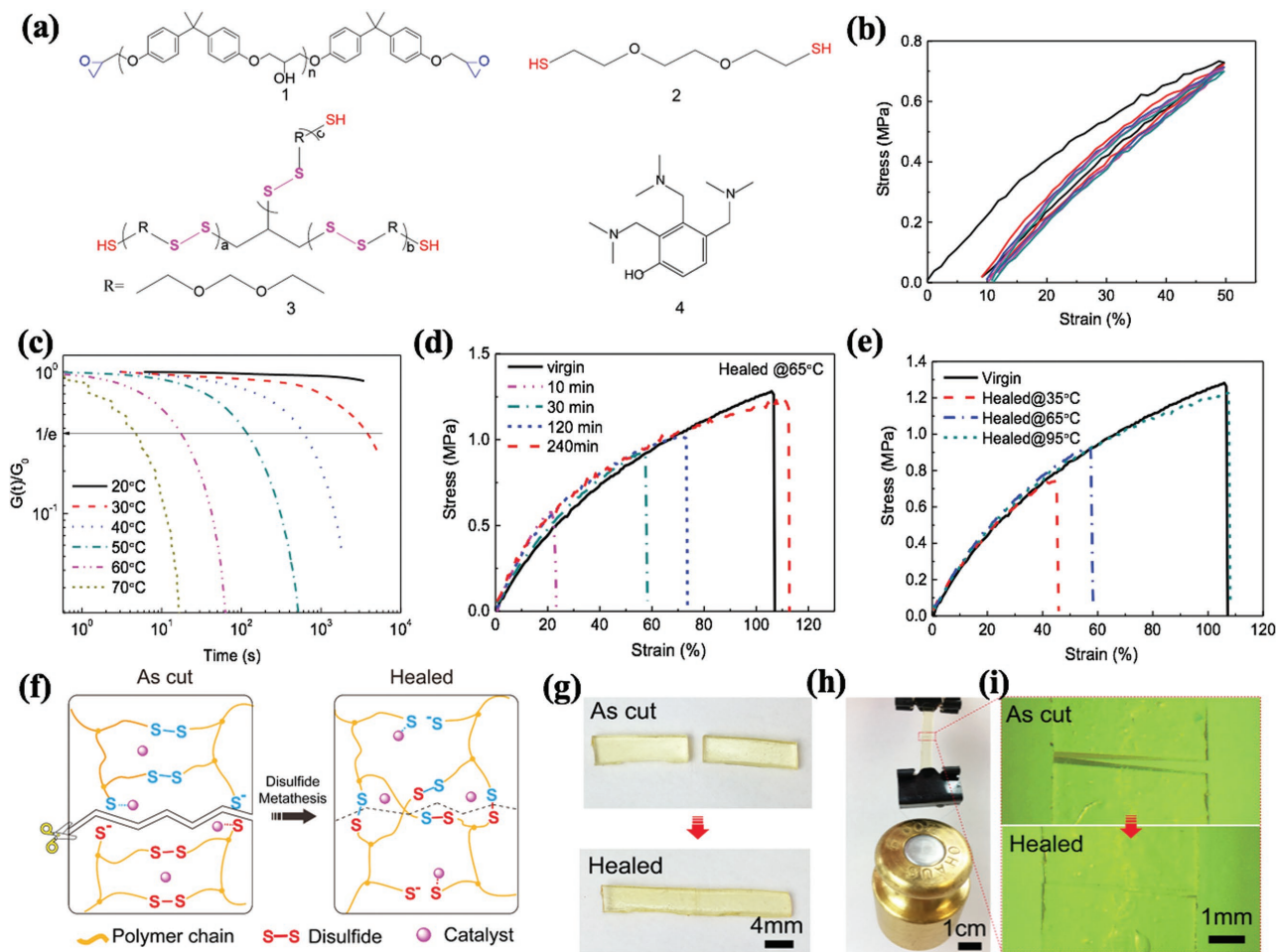


Figure 1. Schematic structure of material design and mechanical healing behavior characterization. a) Chemical structures of starting materials used to prepare vitrimer elastomer. **1** is bisphenol A diglycidyl ether epoxy oligomer; **2** is 2-(ethylenedioxy) diethanethiol used as a spacer; **3** is polysulfide oligomer as a crosslinker, and **4** is 2,4,6-tris(dimethylaminomethyl) phenol used as a curing catalyst. b) Tension stress–strain behavior of the vitrimer elastomer for five repeated cycles. c) Normalized stress relaxation curves of vitrimer elastomer at different temperatures. d) Typical tensile stress–strain curves of virgin and healed vitrimer elastomer at 65 °C for different time. e) Typical tensile stress–strain curves of virgin and healed vitrimer elastomer at different temperatures for 30 min. f) Schematic illustration of self-healing process by disulfide metathesis catalyzed by an organic base in a vitrimer elastomer network. g) The images showing the typical self-healing behavior: a rectangular sample was first cut by blade then healed at 95 °C for 20 min. h) The healed sample can load 200 g of weight. i) Optical microscope image of as-cut crack and healed sample.

time of 30 min, the healing efficiency is 45% at 35 °C, which increases to nearly 100% at 95 °C. Figure 1f shows the proposed healing mechanism by disulfide metathesis in the polysulfide network. Transient states are formed between the catalyst and disulfide bonds resulting in ion-pair intermediates consisting of thiolate anions.^[26] As the bond exchange reaction proceeds, constant reshuffling of the molecular chains leads to rearrangement of the network structure. The healing efficiency is determined by the network rearrangement behavior as indicated by the stress relaxation capability. Higher temperature indicates faster network rearrangement leading to higher healing efficiency for the same healing time (Figure S6, Supporting Information). Longer healing time results in higher probability to reform disulfide linkages between the crack surfaces contributing to better recovery at the same healing temperature (Figure S7, Supporting Information). It should be noted that the amount of disulfide bond is high (22 wt%) in this vitrimer

material and the weak disulfide bond would break before other covalent bonds under external stress upon cut or damages.^[27] With excellent capability to reform the dynamic disulfide bond between the crack surfaces, nearly 100% of the healing efficiency can be obtained for the vitrimer here.

To visually demonstrate the healing event, a rectangular strip was cut and healed to load weight. The sample was cut by a sharp blade, and then the crack surfaces were put together followed by treating at 95 °C for 20 min. It was shown that the healed sample could retain satisfactory stretchability (Figure 1g; Movie S1, Supporting Information). Optical microscopy images show that the crack was healed. It should be mentioned that the sample could also be healed by exposure to intense pulsed light (IPL), which dramatically decreases the duration of the healing process (Movie S2, Supporting Information). After only 30 s of IPL treatment, the sample can regain its original mechanical properties. Thermal images (Figure S8, Supporting Information) revealed

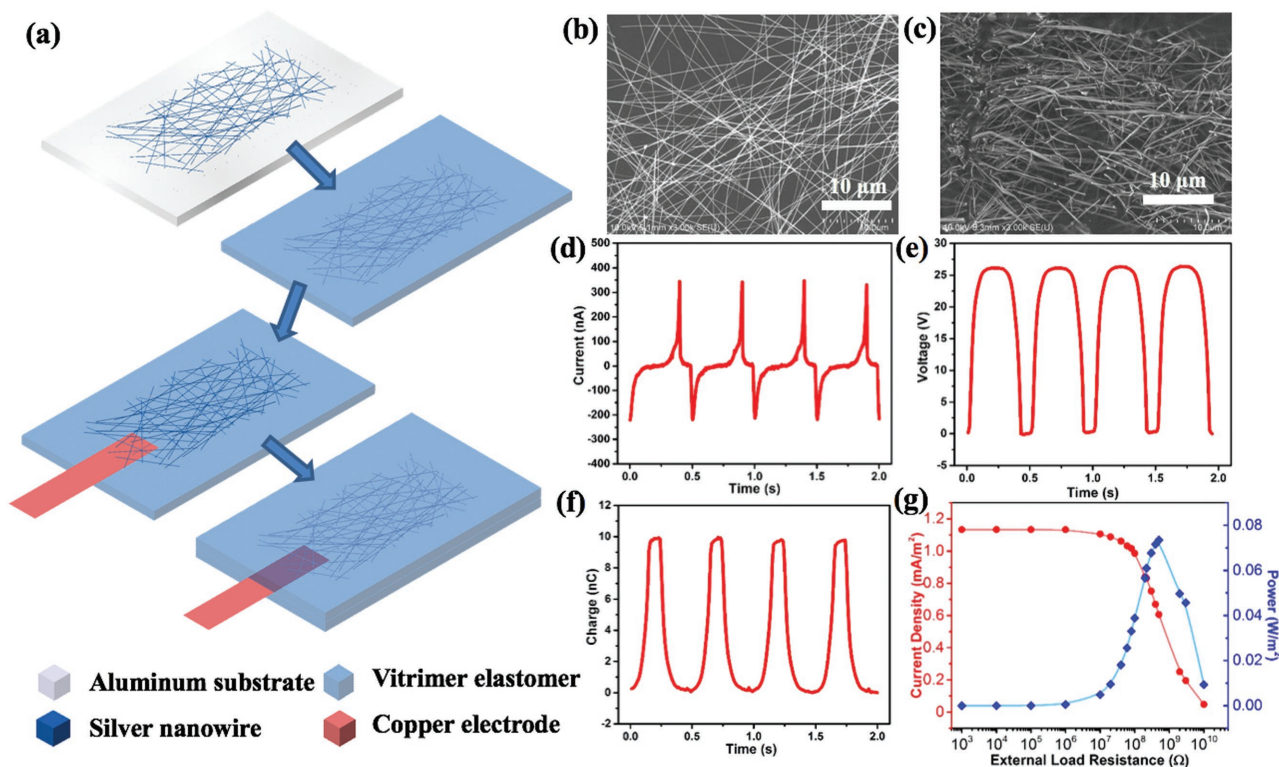


Figure 2. Schematic fabrication process of VTENG and basic electrical output characteristics. a) Schematic diagram of VTENG fabrication process. Scanning electron microscope (SEM) images of silver nanowire conducting network b) on substrate and c) on the surface of elastomer. d) Short-circuit current I_{SC} , e) open circuit voltage V_{OC} , and f) short-circuit transferred charge Q_{SC} of the VTENG. g) Variation of the output current density and power density with different external load resistances.

that high temperature can be generated by IPL irradiation in just few seconds so the recovery process starts almost instantly, enabling scratches, cracks, and even breaks to be repaired at extreme high speed (Figure S9, Supporting Information).

The vitrimer elastomer was utilized as a matrix to construct TENG devices. The basic VTENG fabrication process is depicted in Figure 2a. Ice pop-like architecture was adopted in the design of the mechanical energy harvester/sensor. Percolating silver nanowire networks were embedded in the vitrimer elastomer as the electrode, and copper tape was attached and extended out of the elastomer for the convenience of measurement. Randomly arranged silver nanowires ($L \approx 120 \mu\text{m}$; $W \approx 120 \text{ nm}$; Figure S10, Supporting Information) cast on the substrate established a good conductive network on the 2D plane (Figure 2b). As the network was percolated into the elastomer, a 3D conductive network was formed in the VTENG. As shown in Figure 2c, the silver nanowire network was merged with the elastomer and the nanowires were tightly interconnected, providing more freedom when the electrode was suffering stress. The resultant electrode possessed excellent connectivity not only under unstrained conditions but also under particular strain levels, which made it a superior candidate as the stretchable electrode for VTENG.

The fundamental working mechanism of TENGs is a conjugation of contact electrification and electrostatic induction. Electrostatic charges are first introduced through the contact electrification process between two dissimilar material surfaces, and following separation of the two surfaces by external force, the contact-induced triboelectric charges generate a potential

drop that drives the flow of electrons between two electrodes connected to the surfaces.^[28] Traditional contact-separation mode and sliding-mode TENGs require two electrodes working in pairs while one of them is attached to the mobile part of the device, limiting their applicability in the wearable electronics area. For single electrode mode TENGs, only one electrode is required for collecting electric signals, and the other electrode serves as an electric potential reference which can be placed anywhere in the system, even directly with the ground. Although the charge transfer efficiency η_{CT} (defined as the ratio between the final transferred charges and the total triboelectric charges) of the single electrode mode is lower than the other modes theoretically,^[29] the ability to accommodate to almost any arbitrary surface to harvest mechanical energy as well as better gap tolerance in practical applications compensate greatly for that factor. The working mechanism of the developed VTENG is illustrated in Figure S11 in the Supporting Information.

Typical electrical output was measured and four-cycle raw data is presented in Figures 2d–f. The VTENG (L : 10 cm; W : 3 cm) was placed on a crossed roller bearing stage that was mounted on the optical stage, and a $2 \times 2 \text{ cm}^2$ polytetrafluoroethylene (PTFE) film was attached to the end of a linear motor in order to develop periodical vertical contact with VTENG. Separation distance was set to 40 cm and the contact interval was 0.5 s to achieve a frequency of 2 Hz. The peak short circuit alternating current (I_{sc}) and transferred charge (Q_{sc}) were $\approx 350 \text{ nA}$ and 10 nC, respectively. The open circuit voltage (V_{oc}) nearly reached 26 V. By introducing external load resistance ranging

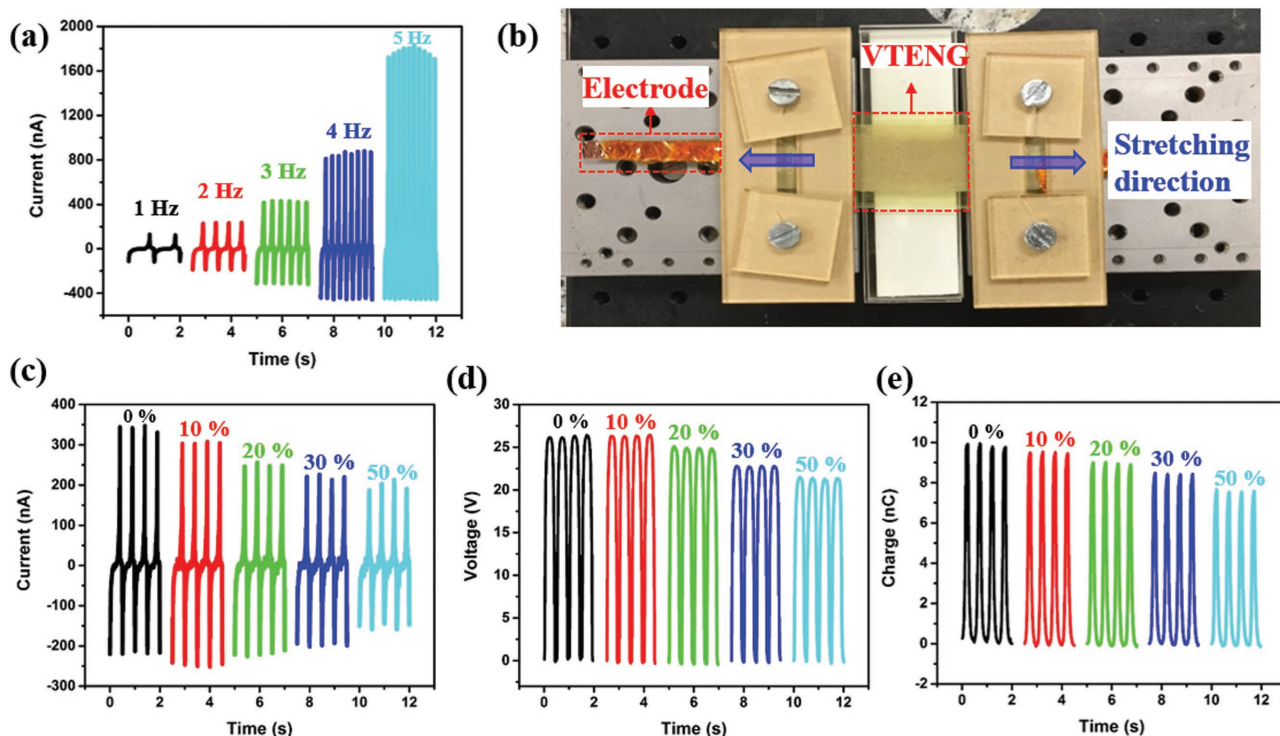


Figure 3. Output characteristics of VTENG under strain. a) I_{SC} of VTENG with different contact frequency. b) Setup for output performance test under strain. c) I_{SC} , d) V_{OC} , and e) Q_{SC} results under strain.

from 1 K Ω to 10 G Ω , a maximum output power density of 0.073 W m⁻² was realized when the load was about 5 G Ω .

In comparison with traditional generator, TENGs have great advantages in scavenging irregular low frequency mechanical energy (1–5 Hz).^[11] Dependence of the short-circuit current on the frequency of original length is presented in Figure 3a. The generated short-circuit current of the VTENG increased as frequency increased, ranging from \approx 130 nA at 1 Hz to \approx 1800 nA at 5 Hz. This is due to the short-circuit current being strongly affected by the velocity, and thus it is proportional to frequency while the separation distance remains constant. We have previously tested the cyclic tensile behavior of the elastomer, which demonstrated its excellent elastic properties. The tensile-strain-dependent output performance is presented in Figure 3. As shown in Figure 3b, the VTENG was deployed on an acrylic-substrate stage, with each end fixed to a double-row steel linear ball-bearing stage and clipped by acrylic blocks. Other device setup parameters were consistent with previous electrical output tests. By adjusting the differential micrometers on the ends of the moving carriages, precise extended distance could be realized in order to calculate the elongation of the VTENG. With the increase of distance between the two bearing stages, the VTENG was uniaxially stretched along the long axis direction. It was observed that there was certain degree of degradation in output performance as the tensile strain increased (Figures 3c–e). I_{SC} , V_{OC} , and Q_{SC} were reduced about 11%, 1%, and 4%, respectively, at a tensile strain of 10%. The main reason for the fall of I_{SC} was the strain-induced lower connectivity in the 3D conductive network. Displacement of silver nanowires in the electrode led to the rise in the internal resistance, which resulted in an increase

of inherent capacitance. Even at 50% tensile strain, the VTENG maintained more than 75% of its original output.

In addition to the good flexibility and stretchability, the most important feature of the vitrimer elastomer-based VTENG is its ability to self-recover. We have demonstrated that the elastomer has a fast healing capability and almost no mechanical degradation with proper stimulation (Figure 1d,e; Movies S1 and S2, Supporting information). In order to characterize the detailed electrical properties, an L-shaped square ruler like VTENG (L: 6 cm; W: 3 cm) was fabricated (Figure 4a). Two electrodes were deployed to test the connectivity and performance of both the original and repaired devices. The strategy is depicted in Figure 4b, in which we used a sharp blade to make two cuts along the edges of the VTENG to make sure that the silver nanowire conducting network was fully disconnected (Figure 4c), as confirmed through optical microscope and scanning electron microscope images (Figure 4d,e). Next, the broken parts were reattached together and treated with thermal stimulation to boost the recovery process. After being heated in an oven at 65 °C for 60 min, the repaired VTENG was removed from heat. Figure 4g shows that the three separated parts rejoined following heat treatment, and the white reflection light on the surface indicates the lack of remarkable scars aside from a small indentation on the previous wound. As shown in Figure 4h, the silver nanowire network in the elastomer was not influenced by the heat treatment and remained abundant and anfractuous. It is also noted that, on the border of two sections, a significantly darker boundary may be observed, which was due to the welding results of the conductive network during the healing process. Silver nanowires that are exposed on the

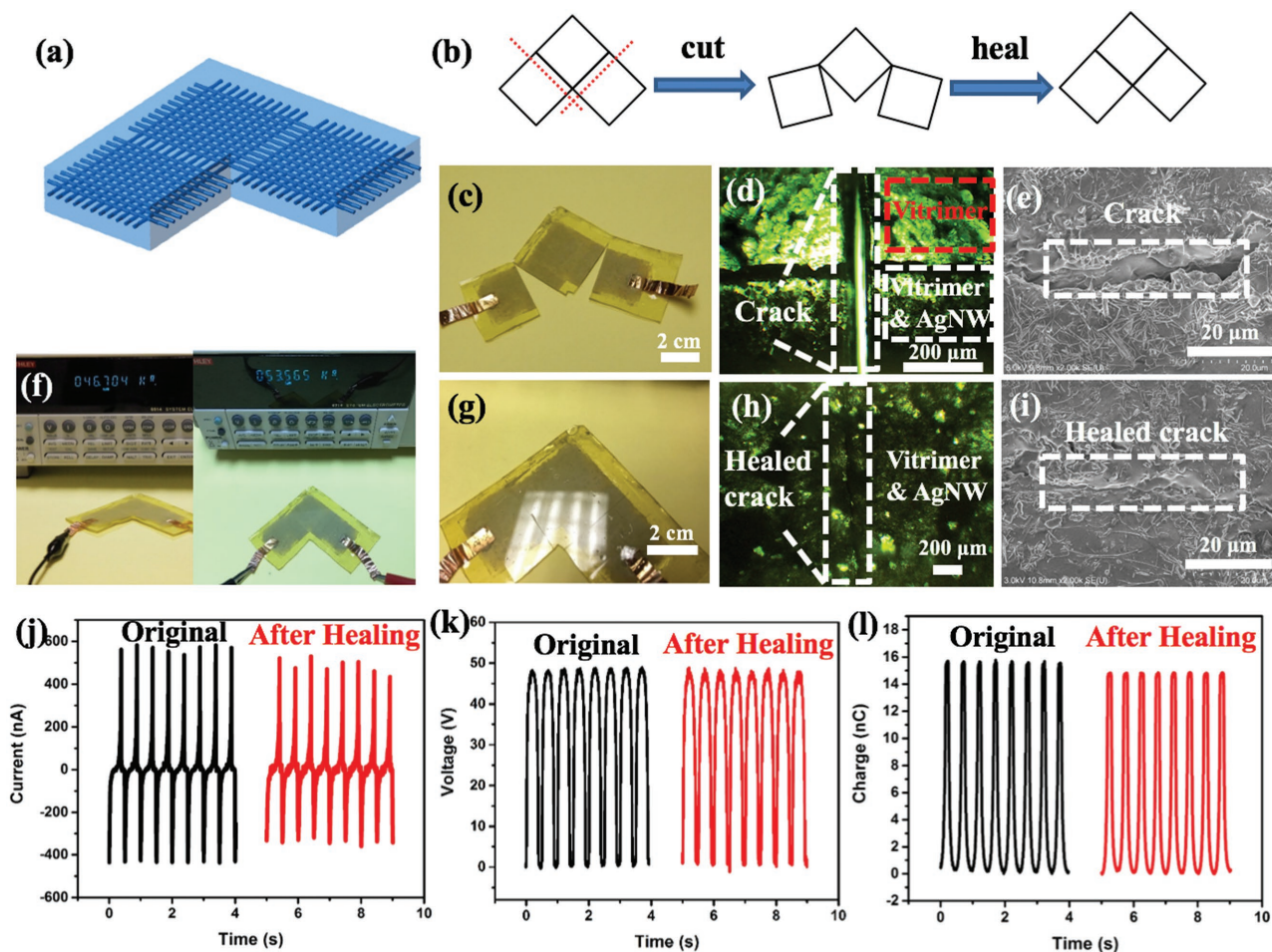


Figure 4. Break and recovery of VTENG and the comparison of output performance. a) Space diagram of the square ruler-like VTENG. b) Strategy for break and recovery. c–e) Photos and g–i) images from optical microscope and scanning electron microscope of broken and recovered VTENG, respectively. f) Resistance between two copper electrodes of original (left) and repaired (right) VTENG. j) I_{SC} , k) V_{OC} , and l) Q_{SC} results of original (black) and repaired (red) VTENG.

fracture surface will reattach to each other in the initial phase of recovery. While the sample was heated, the disulfide bonds in the vitrimer elastomer were boosted, and a cross nucleophilic attack of thiolate anions to other sulfur atoms occurred with the movement of chain segments leading to exchanges of disulfide bonds. As the reaction continued, attached silver nanowires were held tightly by the elastomer. As neighboring molecular chains were constantly reshuffling, a balance was achieved over time, resulting in a rebuilt structure. At the same time, due to the thermal treatment the attached silver nanowires were also welding together, which further recovered the connectivity^[30] (Figure 4i). The connectivity was tested by comparing the variation of resistance change. Figure 4f shows the pictures of resistance of original and repaired devices. The device had an original resistance of ≈ 46.8 k Ω and a repaired resistance of ≈ 53.5 k Ω . The increased resistance resulted from the diminutive damage that the conducting silver nanowire network suffered. Although most of the channels were able to be reconnected, when the dimensions were shrunk down to the nanoscale, a small displacement could be understood to lead to mismatch in some areas. The electrical performance of the

original and repaired VTENGs is compared in Figures 4j–l. The changes in all three electrical output parameters were observed to be insignificant. From the aspect of the fundamental $V-Q-x$ relationship of TENGs,^[31] it is always advantageous for the inherent resistance of TENG to be huge (M Ω to G Ω) or close to infinity in order to maximize the output. Compared with the impedance of normal load conditions, the parasitic resistance from the conductive electrode is also negligible, which explains why resistors are not one of the parameters that the $V-Q-x$ model concerns.^[32] All processes, including the repairing and testing of the VTENG, were recorded in Movie S3 in the Supporting information.

Inspired by the assembly method behind jigsaw puzzles and building blocks toys, and combined with the unique features of vitrimer elastomer, we propose a new approach for TENG fabrication. As shown in Figure 5, a terrace-structured VTENG was designed. The terrace structure further increases the effective contact area of the conducting layer and the overlapping area of the two sections, reducing the possibility of disconnection and making the welding more reliable. The silver nanowire conducting layer was sandwiched between the two layers of

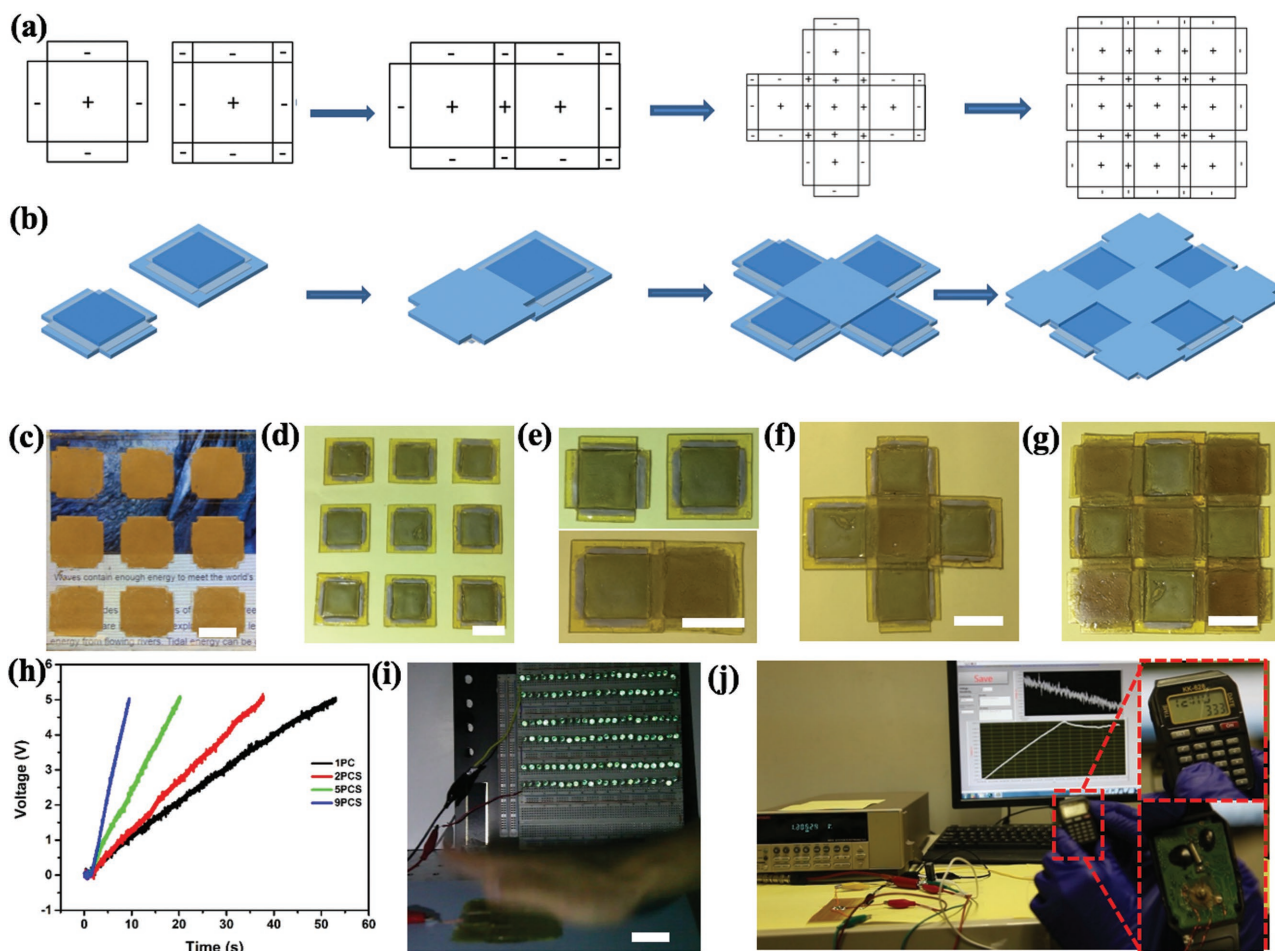


Figure 5. Fabrication method of scalable VTENG and application demonstration. a) Top view, b) space diagram, and c–g) photos of the fabrication method and VTENG assembled with two, five, and nine pieces. h) The charging curve of a $1 \mu\text{F}$ commercial capacitor to 5 V by one, two, five and nine pieces-assembled VTENGs, respectively. Demonstration of i) lighting 150 LEDs at the same time and j) powering a watch with calculator function by the nine-piece assembled VTENG. Scale bar: 3 cm.

1 mm thick vitrimer elastomer, of which the side length of the top and bottom layer were 20 and 30 mm, respectively. Since the conducting layer was cast to an area of $23 \times 23 \text{ mm}^2$, which was smaller than the top layer of polymer, there was an area of $3 \times 23 \text{ mm}^2$ exposed conducting surface on each side. By flipping another block down and clipping them together, the two conducting sections were connected by the overlap of the conducting layer. After being heated at $65 \text{ }^\circ\text{C}$ for 60 min, the two blocks merged into a new VTENG. As shown in Movie S4 in the Supporting information, the two blocks of the new VTENG were tapped using a $20 \times 20 \text{ mm}^2$ PTFE film and the V_{oc} values for both parts were $\approx 25 \text{ V}$, which indicated good connectivity for this extended VTENG. Through repetition of the above procedure, the VTENG area could be extended even further. Figure 5a,b depicts the fabrication strategy from a top view and space diagram. Figure 5a indicates the layer number of the selected section, where “–” and “+” represent single and double layers. Through these means, the VTENG could be further extended. Figure 5c,d depicts the before and after photos of the vitrimer and conducting material tailored into building blocks, and the fabricated VTENGs with two, five, and nine blocks are shown

in Figure 5e,f, respectively. By connecting to a rectifier, the efficiency of charging a $1 \mu\text{F}$ commercial capacitor to 5 V was compared between the VTENGs assembled with one, two, five, and nine pieces (Figure 5h). Human palm tapping at $\approx 3 \text{ Hz}$ was used as a mechanical energy source, and the charging duration time for the aforementioned VTENGs were 53.1, 31.8, 20.3, and 9.5 s, respectively. There was an almost 450% increase in charging efficiency as the VTENG increased from one to nine pieces, which exhibited significant enhancement in energy conversion through the terrace assembly. The main reason for enhanced efficiency was the increase in effective contact area, which is the most critical parameter in charge induction, meaning the output of the extended VTENG was expected to increase several times from one to nine pieces. The power that was generated from the nine-piece assembled VTENG can light up to 150 green light-emitting diodes (LED) (Figure 5i; Movie S5, Supporting Information). When connected to a rectifier and a $100 \mu\text{F}$ commercial capacitor, the nine-piece VTENG provided sustainable energy to drive a wearable watch with calculator function. The electricity converted from palm tapping could not only satisfy the simple I/O system functionality but also provide

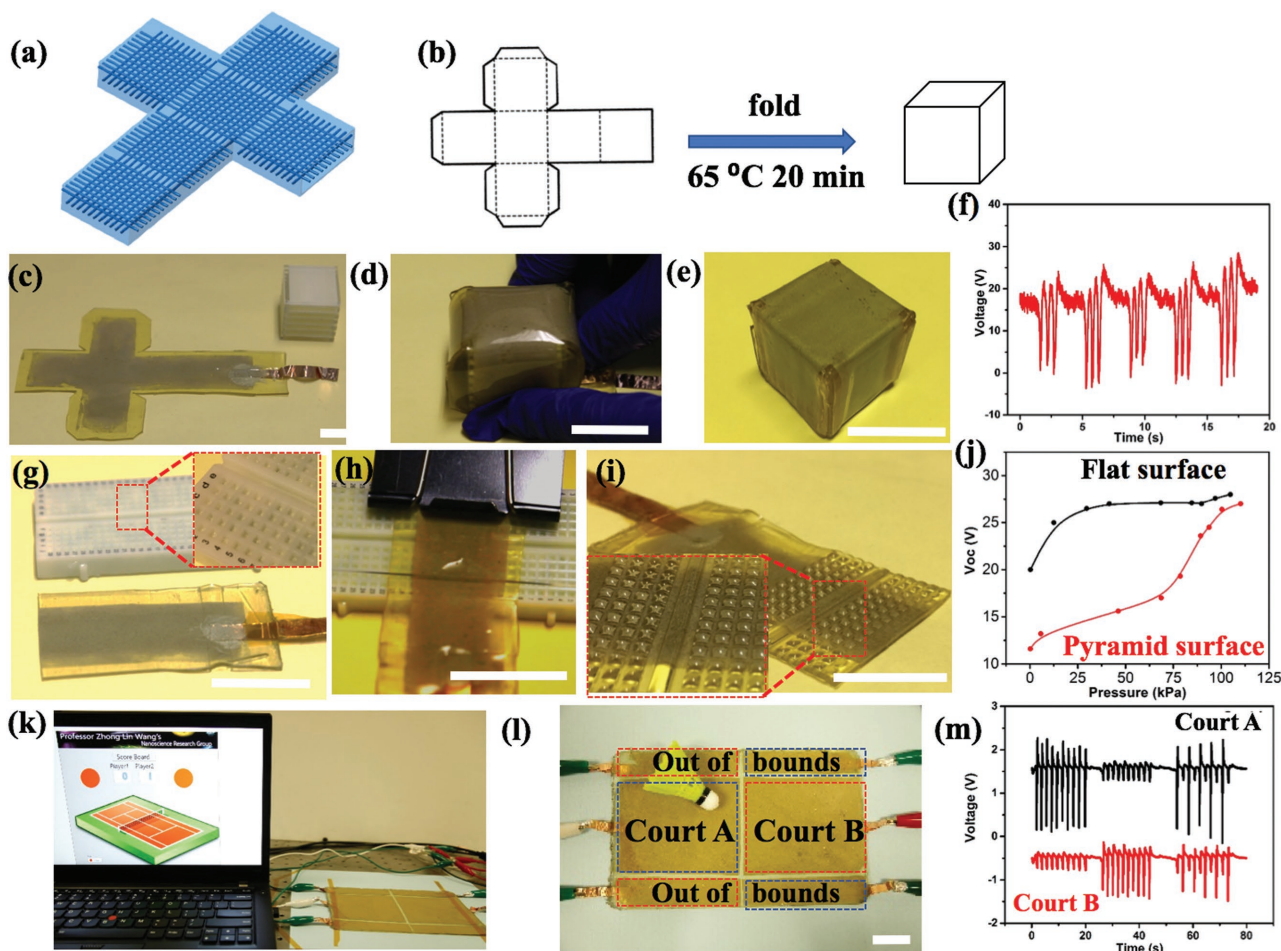


Figure 6. Demonstration of converting VTENG from 2D to 3D and corresponding pressure/tactile sensing. a) Space diagram of the cross-shaped VTENG. b) Strategy for converting VTENG from 2D to 3D. c) The 2D in plane VTENG was folded into d) a cube through an origami method. After treating at 65 °C for 20 min. e) VTENG was competently accommodated to the surface of the cube. f) Voltage signal of five faces of the 3D VTENG. g–i) Fabrication method of developing sensing elements on existing VTENG surfaces. j) V_{oc} comparison of VTENG with and without sensing elements. k) Self-powered badminton sensing court and scoring system and l) court division illustration. m) Real-time voltage signal when balls fall onto different courts. Scale bar: 3 cm.

the capacity for complicated data processing, such as, accurate multiplication and division (Movie S6, Supporting Information). Once the capacitor was charged to 1.5 V, the watch was able to be boot up and remained functional with the energy converted from constant palm tapping (Figure S12, Supporting Information).

Aside from these numerous mentioned features, the VTENG also possessed favorable conformability to various arbitrary surfaces and adaptively from 2D to 3D.^[33] We designed a cross-shaped VTENG (Figure 6a) and tailored it to the extended surface of a $30 \times 30 \times 30 \text{ mm}^3$ cube (Figure 6c). Through folding it up with a cubic filler inside and following the origami method (Figure 6d), the in-plane 2D VTENG was then transformed into a 3D VTENG (Figure 6e) after heat treatment at 65°C for 20 min. Taking a closer look at the as achieved 3D VTENG, the planes on each side were perfectly attached to the surface of the cubic filler. It should be noted that during the whole process, no glue or additional adhesives were used. This is mainly attributed to the bond exchange reaction of the vitrimer elastomer. With the increase of temperature, the

relaxation activation energy was elevated. The stress relaxation modulus and τ decreased sharply with increasing temperature. High τ in low temperature ensured the stability and elasticity of VTENG, while low τ in high temperature enabled the conformability and healing ability. The VTENG was softened first at lower temperatures, and as it gained enough energy to activate the bond exchange reaction, the neighboring attached interfaces merged together into a unified body. Through this process, the 2D VTENG was then converted to a 3D VTENG. We further measured the V_{oc} of the 3D VTENG through tapping with a PTFE film, and found that a stable voltage of about 40 V can be achieved (Figure 6f). This indicates that although severe deformation was suffered, the 3D VTENG still maintained satisfactory sensitivity to external motion. Fabrication and testing processes were recorded in Movie S7 in the Supporting Information. Due to the VTENG's excellent surface adaptivity and deformability, the arduous task of achieving these factors in wearable electronic device fabrication may be alleviated now. Figure 6g–j demonstrate a new approach to develop a pyramidal structure on existing VTENG surfaces using a reverse mold

method, which imbues the VTENG with pressure-sensing capacity. A VTENG with the desired area for sensing elements was mounted on a reverse pyramid mold and supported with a glass sheet. After treating at 65°C for 20 min, pyramidal structural arrays were successfully developed on the VTENG surface (Figure 6i; Movie S8, Supporting Information). For the original VTENG with smooth surfaces, the V_{oc} saturated quickly to 28 V when the pressure reached 40 kPa (Figure 6j). However, for the VTENG with sensing elements, the V_{oc} gradually increased from 0 to 70 kPa, and an abrupt slope was observed from 80 to 100 kPa. The difference in V_{oc} for the two devices resulted from different effective contact areas under various pressures. For the original smooth-surfaced VTENG, the contact between the surface and objects was unhindered, and all force was directly applied to the corresponding area. In that case, as long as the object maintained full contact with the surface, the V_{oc} could saturate to the maximum value rapidly. For the VTENG with patterned pyramidal structures on the surface, the force coming from an object would be hindered by the protrusions first. As the force increases, the pyramidal structures would be pressed so the effective contact area would be closer to the area of the contacting object, and the V_{oc} would increase correspondingly and present a step growth characteristic before becoming saturated. These uniquely structured VTENGs, if fabricated in larger scales, can act as an electronic skin (Figure S13, Supporting Information) and self-powered sensing system. Finally, a self-powered badminton sensing court and scoring system was developed (Figure 6k). As shown in Figure 6l, VTENG was divided into six sections, and Courts A and B were the main playing fields of Players 1 and 2, respectively. Player 1 scored when the shuttlecock fell on Player 2's main court field or when Player 2 made the shuttlecock go out of bounds, and Player 2 scored vice versa (Movie S9, Supporting Information). Figure 6m shows the voltage variations when the shuttlecock fell onto different courts. Real-time signals could be detected and analyzed from the court. If one signal goes beyond the threshold value, immediate analysis will be conducted by the system. By processing it through an analyzing system, an instantaneous judgment may be made and the results will be displayed on the screen simultaneously. What's more, score controversies under dubious circumstances could be eliminated. Accurate results are achieved by simply comparing the signals on both sides of the bound, and reviewing the playback footage or deploying expensive hawk-eye systems are no longer required. It is worth noting that such a sensing system does not require any powering supplies on the sensing end, and due to the self-healing feature of vitrimer elastomers, it can be easily maintained or repaired under a low budget as well.

In summary, a self-healable, flexible, and deformable mechanical energy harvester/sensor was achieved by combining a vitrimer elastomer with a silver nanowire conducting network based on the single electrode mode of triboelectric nanogenerator. Due to the dynamic disulfide exchange reaction in the vitrimer elastomer, the device possesses a series of fascinating features like excellent elasticity/stretchability, outstanding conformability/deformability, and fast scratch or break recovery under thermal or IPL stimulation. The electrical performance can be restored after repairing damage, even after suffering severe deformation. In combination with these features and a

terrace structure, a jigsaw puzzle-like TENG was developed. We demonstrated that the VTENG could be deployed as an energy harvester and tactile/pressure sensor. The significance behind the VTENG is not only a newly developed mechanical energy harvester but also the provision of a facile approach for the fabrication of flexible electronic systems. Devices can be welded and scaled up like jigsaw puzzles and building blocks, while scaling up the electric output performance as well. We can design the shape and morphology by tailoring the body and reforming the surface on demand, and even fabrication of 3D structures can be simplified through an origami strategy. Only basic blocks with various shape and function need to be manufactured, and no molds are required on the user end. Various categories of electrical components like sensors, batteries, or even transistors can be integrated, and the VTENG's functionalities can be extended even more in the near future. The adoption of smart polymers in electronic devices may provide a new route for flexible device fabrication and promote the prosperous development of smart wearable electronics.

Supporting Information

Supporting Information is available from the Wiley Online Library or from the author.

Acknowledgements

J.D., X.K., and R.L. contributed equally to this work. Research was supported by the Hightower Chair foundation, the "thousands talents" program for pioneer researcher and his innovation team. J.D. and R.L. would like to thank the support from the China Scholarship Council. X.K. and H.J.Q. thank the support from a grant by US National Science Foundation (CMMI-1404627).

Conflict of Interest

The authors declare no conflict of interest.

Keywords

flexible, self-powered sensor, triboelectric nanogenerators, vitrimers

Received: October 11, 2017

Revised: November 17, 2017

Published online:

- [1] J. Xu, S. Wang, G.-J. N. Wang, C. Zhu, S. Luo, L. Jin, X. Gu, S. Chen, V. R. Feig, J. W. To, *Science* **2017**, 355, 59.
- [2] W. Gao, S. Emaminejad, H. Y. Y. Nyein, S. Challa, K. Chen, A. Peck, H. M. Fahad, H. Ota, H. Shiraki, D. Kiriya, *Nature* **2016**, 529, 509.
- [3] L.-F. Chen, Z.-H. Huang, H.-W. Liang, W.-T. Yao, Z.-Y. Yu, S.-H. Yu, *Energy Environ. Sci.* **2013**, 6, 3331.
- [4] R. Liu, J. Wang, T. Sun, M. Wang, C. Wu, H. Zou, T. Song, X. Zhang, S.-T. Lee, Z. L. Wang, *Nano Lett.* **2017**, 17, 4240.
- [5] a) Y. Yang, G. Zhu, H. Zhang, J. Chen, X. Zhong, Z.-H. Lin, Y. Su, P. Bai, X. Wen, Z. L. Wang, *ACS Nano* **2013**, 7, 9461;

- b) Y. Xi, H. Guo, Y. Zi, X. Li, J. Wang, J. Deng, S. Li, C. Hu, X. Cao, Z. L. Wang, *Adv. Energy Mater.* **2017**, *7*, 1602397.
- [6] a) Z. L. Wang, T. Jiang, L. Xu, *Nano Energy* **2017**, *39*, 9; b) Z. L. Wang, *Nature* **2017**, *542*, 159.
- [7] J. Chen, G. Zhu, W. Yang, Q. Jing, P. Bai, Y. Yang, T. C. Hou, Z. L. Wang, *Adv. Mater.* **2013**, *25*, 6094.
- [8] a) S. Niu, X. Wang, F. Yi, Y. S. Zhou, Z. L. Wang, *Nat. Commun.* **2015**, *6*, 8975; b) J. Wang, S. Li, F. Yi, Y. Zi, J. Lin, X. Wang, Y. Xu, Z. L. Wang, *Nat. Commun.* **2016**, *7*, 12744.
- [9] a) S. Niu, S. Wang, Y. Liu, Y. S. Zhou, L. Lin, Y. Hu, K. C. Pradel, Z. L. Wang, *Energy Environ. Sci.* **2014**, *7*, 2339; b) Y. Mao, D. Geng, E. Liang, X. Wang, *Nano Energy* **2015**, *15*, 227.
- [10] S. Niu, S. Wang, L. Lin, Y. Liu, Y. S. Zhou, Y. Hu, Z. L. Wang, *Energy Environ. Sci.* **2013**, *6*, 3576.
- [11] Y. Zi, H. Guo, Z. Wen, M.-H. Yeh, C. Hu, Z. L. Wang, *ACS Nano* **2016**, *10*, 4797.
- [12] a) Y. C. Lai, J. Deng, S. Niu, W. Peng, C. Wu, R. Liu, Z. Wen, Z. L. Wang, *Adv. Mater.* **2016**, *28*, 10024; b) X. Pu, M. Liu, X. Chen, J. Sun, C. Du, Y. Zhang, J. Zhai, W. Hu, Z. L. Wang, *Sci. Adv.* **2017**, *3*, e1700015; c) F. Yi, X. Wang, S. Niu, S. Li, Y. Yin, K. Dai, G. Zhang, L. Lin, Z. Wen, H. Guo, *Sci. Adv.* **2016**, *2*, e1501624; d) J. H. Lee, R. Hinchet, S. K. Kim, S. Kim, S.-W. Kim, *Energy Environ. Sci.* **2015**, *8*, 3605.
- [13] a) M. D. Hager, P. Greil, C. Leyens, S. van der Zwaag, U. S. Schubert, *Adv. Mater.* **2010**, *22*, 5424; b) J. L. Mynar, T. Aida, *Nature* **2008**, *451*, 895.
- [14] W. Denissen, J. M. Winne, F. E. Du Prez, *Chem. Sci.* **2016**, *7*, 30.
- [15] a) K. K. Oehlenschlaeger, J. O. Mueller, J. Brandt, S. Hilf, A. Lederer, M. Wilhelm, R. Graf, M. L. Coote, F. G. Schmidt, C. Barner-Kowollik, *Adv. Mater.* **2014**, *26*, 3561; b) X. Kuang, G. M. Liu, X. Dong, X. G. Liu, J. J. Xu, D. J. Wang, *J. Polym. Sci., Part A: Polym. Chem.* **2015**, *53*, 2094.
- [16] a) Y. Amamoto, J. Kamada, H. Otsuka, A. Takahara, K. Matyjaszewski, *Angew. Chem., Int. Ed.* **2011**, *50*, 1660; b) G. Deng, F. Li, H. Yu, F. Liu, C. Liu, W. Sun, H. Jiang, Y. Chen, *ACS Macro Lett.* **2012**, *1*, 275; c) Z. Q. Lei, H. P. Xiang, Y. J. Yuan, M. Z. Rong, M. Q. Zhang, *Chem. Mater.* **2014**, *26*, 2038; d) A. Rekondo, R. Martin, A. Ruiz de Luzuriaga, G. Cabañero, H. J. Grande, I. Odriozola, *Mater. Horiz.* **2014**, *1*, 237.
- [17] P. Taynton, K. Yu, R. K. Shoemaker, Y. Jin, H. J. Qi, W. Zhang, *Adv. Mater.* **2014**, *26*, 3938.
- [18] a) D. Montarnal, M. Capelot, F. Tournilhac, L. Leibler, *Science* **2011**, *334*, 965; b) K. Yu, Q. Shi, M. L. Dunn, T. J. Wang, H. J. Qi, *Adv. Funct. Mater.* **2016**, *26*, 6098.
- [19] a) Y.-X. Lu, Z. Guan, *J. Am. Chem. Soc.* **2012**, *134*, 14226; b) Y.-X. Lu, F. Tournilhac, L. Leibler, Z. Guan, *J. Am. Chem. Soc.* **2012**, *134*, 8424.
- [20] S. P. Black, J. K. M. Sanders, A. R. Stefankiewicz, *Chem. Soc. Rev.* **2014**, *43*, 1861.
- [21] W. Zou, J. Dong, Y. Luo, Q. Zhao, T. Xie, *Adv. Mater.* **2017**, *29*, 1606100.
- [22] a) L. Sheng, Y. Liang, L. Jiang, Q. Wang, T. Wei, L. Qu, Z. Fan, *Adv. Funct. Mater.* **2015**, *25*, 6545; b) C. Wang, H. Shen, Y. Tian, Y. Xie, A. Li, L. Ji, Z. Niu, D. Wu, D. Qiu, *ACS Appl. Mater. Interfaces* **2014**, *6*, 13061.
- [23] B. C. Tee, C. Wang, R. Allen, Z. Bao, *Nat. Nanotechnol.* **2012**, *7*, 825.
- [24] a) C. S. Luo, P. Wan, H. Yang, S. A. A. Shah, X. Chen, *Adv. Funct. Mater.* **2017**, *27*, 1606339; b) T.-P. Huynh, P. Sonar, H. Haick, *Adv. Mater.* **2017**, *29*, 1604973.
- [25] X. Kuang, G. Liu, X. Dong, D. Wang, *Mater. Chem. Front.* **2017**, *1*, 111.
- [26] C. e. Yuan, M. Z. Rong, M. Q. Zhang, Z. P. Zhang, Y. C. Yuan, *Chem. Mater.* **2011**, *23*, 5076.
- [27] A. Ruiz de Luzuriaga, J. M. Matxain, F. Ruiperez, R. Martin, J. M. Asua, G. Cabanero, I. Odriozola, *J. Mater. Chem. C* **2016**, *4*, 6220.
- [28] G. Zhu, C. Pan, W. Guo, C.-Y. Chen, Y. Zhou, R. Yu, Z. L. Wang, *Nano Lett.* **2012**, *12*, 4960.
- [29] S. Niu, Z. L. Wang, *Nano Energy* **2015**, *14*, 161.
- [30] J. Li, J. Liang, L. Li, F. Ren, W. Hu, J. Li, S. Qi, Q. Pei, *ACS Nano* **2014**, *8*, 12874.
- [31] S. Niu, Y. Liu, S. Wang, L. Lin, Y. S. Zhou, Y. Hu, Z. L. Wang, *Adv. Mater.* **2013**, *25*, 6184.
- [32] S. Niu, Y. Liu, Y. S. Zhou, S. Wang, L. Lin, Z. L. Wang, *IEEE Trans. Electron Devices* **2015**, *62*, 641.
- [33] a) Y. Liu, J. Genzer, M. D. Dickey, *Prog. Polym. Sci.* **2016**, *52*, 79; b) H. Ko, A. Javey, *Acc. Chem. Res.* **2017**, *50*, 691.